The DOI for this manuscript is doi: 10.1175/BAMS-D-15-00324.1

The final published version of this manuscript will replace the preliminary version at the above DOI once it is available.

If you would like to cite this EOR in a separate work, please use the following full citation:

Huntington, J., K. Hegewisch, B. Daudert, C. Morton, J. Abatzoglou, D. McEvoy, and T. Erickson, 2017: Climate Engine: Cloud Computing and Visualization of Climate and Remote Sensing Data for Advanced Natural Resource Monitoring and Process Understanding. Bull. Amer. Meteor. Soc. doi:10.1175/BAMS-D-15-00324.1, in press.

# Climate Engine: Cloud Computing and Visualization of Climate and Remote Sensing Data for Advanced Natural Resource Monitoring and Process Understanding

Justin L. Huntington[1], Katherine C. Hegewisch[2], Britta Daudert[1], Charles G. Morton[3], John T. Abatzoglou[2], Daniel J. McEvoy[1], Tyler Erickson[4]

[1]Western Regional Climate Center, Desert Research Institute, Reno, NV
[2]Department of Geography, University of Idaho, Moscow, ID
[3]Division of Earth and Ecosystem Science, Desert Research Institute, Reno, NV
[4]Google, Inc, Mountain View, CA

Keywords: cloud computing, climate, meteorology, remote sensing, web visualization, Google Earth Engine

Submitted to the Bulletin of the American Meteorological Society on October 11, 2016

Corresponding author: Justin Huntington, Desert Research Institute, 2215 Raggio Parkway, Reno, Nevada, 89512;
Email: justin.huntington@dri.edu; Phone: 775-673-7670

**Abstract**

The paucity of long-term observations, particularly in regions with heterogeneous climate and land cover, can hinder incorporating climate data at appropriate spatial scales for decision-making and scientific research. Numerous gridded climate, weather, and remote sensing products have been developed to address the needs of both land managers and scientists, in turn enhancing scientific knowledge and strengthening early warning systems. However, these data remain largely inaccessible for a broader segment of users given the computational demands of big data. Climate Engine (ClimateEngine.org) is a web-based application that overcomes many computational barriers users face by employing Google's parallel cloud computing platform, Google Earth Engine, to process, visualize, download, and share climate and remote sensing datasets in real-time. The software application development and design of Climate Engine is briefly outlined to illustrate the potential for high-performance processing of big data using cloud computing. Secondly, several examples are presented to highlight a range of climate research and applications related to drought, fire, ecology, and agriculture that can be rapidly generated using Climate Engine. The ability to access climate and remote sensing data archives with on-demand parallel cloud computing has created vast opportunities for advanced natural resource monitoring and process understanding.

**Capsule Summary**

Climate Engine enables users to process, visualize, download, and share climate and remote sensing datasets with a simple web-connection, thereby overcoming common big data barriers.

## Introduction

Climate and weather affect all sectors of society at regional to local scales. However, the paucity of long-term observations in many parts of the globe provides a constraint on the utilization of data for applied use and scientific research. To address the need for place-based data, a number of operational gridded climate and meteorological datasets have been created (Daly, 1994; Mitchell, 2004; Abatzoglou, 2013; Thornton et al., 2014; Oyler et al., 2014), in addition to remote sensing datasets that are freely available and being increasingly used. However, the accessibility of these data to researchers, decision makers, and the general public are limited due challenges related to computational requirements, data storage, and software needed to work with large data volumes.

A good example of these limitations can be illustrated with current drought monitoring. Climate data are the primary basis for operationally providing information about the degree and intensity of drought conditions through the use of drought indices (Hobbins et al., 2016; Svoboda et al., 2002; McKee et al., 1993). Climate based drought indices are complemented by relatively fine resolution satellite remote sensing data (Anderson et al., 2007a,b; Brown et al., 2008; Wang and Qu, 2007). These data can be calculated at their native spatial and temporal resolutions - often at spatial scales from 30-m to 12-km and temporal scales from hourly to weekly. However, operational products that are summarized for decision makers are typically available at much coarser spatial (e.g., climate division) and temporal (e.g., monthly) resolution. Moreover, many operational web-based products are static, and offer limited options for interacting with the data, customizing analyses to specific time periods for summaries, or acquiring the digital data.

Recognizing these limitations, recent web applications have focused on providing on-demand and dynamic visualization, extraction, and processing of pre-computed data (Berrick et al., 2009; Eberle et al., 2013; Teng et al., 2016). New computing technologies, where massively parallel processors are co-located with data collections, allow for on-demand and on-the-fly generation of custom data products and visualization, thereby avoiding many limitations of the past (Moore and Hansen, 2011; Baumann et al., 2016; Yang et al., 2017). The development of a cloud computing web application for on-demand processing and visualizing climate and remote sensing data is motivated by current web application limitations, and by climate and natural resource scientist and manager needs related to drought, ecology, and agriculture that can be addressed through advanced processing and visualization of earth observation archives.

This article outlines the development of a free web application called Climate Engine (http://ClimateEngine.org) (Figure 1) that uses Google's parallel cloud computing platform, Google Earth Engine, to enable users to process, visualize, download, and share various global and regional climate and remote sensing datasets and products (e.g. anomaly maps and time series) in real-time. Climate Engine helps overcome many of the data storage and processing limitations that are common to researchers, practitioners, and stakeholders. The development of Climate Engine is detailed through a brief discussion of the software application development and design. Several case study applications of Climate Engine are highlighted to illustrate its ability to generate maps and time series for rapid analysis and visualization, and to support advanced natural resource monitoring and process understanding.

## Methods

The Climate Engine web application development and design philosophy was centered around providing the ability for users to perform on-demand mapping and time series visualization and analyses that are customizable, and where map and time series results can be downloaded in common file formats, or shared via web URL links (see sidebar for Application and Development Design details). Datasets and variables available within Climate Engine are derived from existing Google Earth Engine image collections that are consistently updated with minimal latency (approximately 1 to 16-days) operational data (Table 1). Additional datasets, variables, and calculations are continually being added by user request and as Climate Engine evolves.

Climate Engine offers both mapping and time series analysis options. Users are able to choose specific product types (remote sensing or climate), data sets (different satellite platforms or gridded climate datasets), variables (from precipitation to vegetation indices), and common calculations (climatologies or anomalies) and statistics (mean, median, max, min, total) for customized time periods. In the mapping view, users are able to modify the map layer displayed on the Google map by adjusting the color palette, transparency, and value ranges, perform masking, or add vector layers to the map. Users can also request values from the map or download rectangular regions of the map layer in GeoTiff format (Figure 1). In the time series view, users are able to choose from one of three types of time series visualizations for data covering either a point location or an area-average: daily values (or native temporal resolution of dataset), interannual summaries of values over a defined period, or values within a year compared to statistics from other years. Data from multiple point locations or from multiple variables can be compared at the same time. Users can dynamically interact with the resulting scalable vector graphics (SVG) figure to view values at data points, zoom in on the time series figure, toggle the display of series data, download the figure in common image formats, and download the data in .csv or .xls file format. Climate Engine provides easy access to remote sensing and climate archives by pairing cloud computing capabilities and a web application, thereby avoiding the computational expenses of storage and processing such large datasets.

## Case Study Applications

We demonstrate the potential of Climate Engine to both the research community and decision makers by highlighting several recent case studies related to climate, drought, fire, ecology, and agriculture. Map and time series figures shown in the case studies were all computed and downloaded using Climate Engine, and edited (i.e. projection and color modifications) to create publication quality graphics; however, readers can visit ClimateEngine.org/BAMS to replicate these case study maps and time series in real-time.

### ***Climate***

Recent winters have featured a pattern of anomalously warm air over the Arctic and anomalously cool temperatures over portions of mid-latitude continents, potentially a by-product of arctic sea-ice loss and internal atmospheric variability that has been called the “polar vortex” (Overland and Wang, 2016; Waugh et al., 2016). For example, the Arctic-wide temperature anomaly in January-February 2016 was 5.0$^{o}$C above normal (Overland and Wang, 2016), whereas the eastern half North America was exceptionally cool. Climate observations are rather sparse in the Arctic. However, fine scale (1-km) temperature anomalies can be detected through remotely sensed land surface temperature (LST), from the MODIS sensor, onboard NASA's Terra and Aqua satellites. Climate Engine's mapping tools were used to compute and visualize anomalous surface temperature and snow cover maps in the following examples. Figure 2a illustrates the median LST anomaly for January - February 2016 relative to a 2000-2015 baseline climatology, showing large swath of Alaska, Canada, Greenland, and Siberia with LST from 6-10$^{o}$C above normal. Figure 2b highlights a similar example, but for JFM 2015, where the impact of the polar vortex on LST is clear and compelling.

Lastly, Greenland experienced unusually high LST in April 2016, with some locations in the interior approaching 20$^{o}$C above the 2000-2015 average (Figure 2c), prompting an early commencement for ice melt in the south-western portion of Greenland in mid-April that resulted in widespread ice loss (Mottram, 2016). Figure 2d shows the unusually low ice cover (via NDSI from MODIS) in early April along the southwest portion of the Greenland ice sheet and coincides with early melting (Mottram, 2016).

***Drought***

Drought is a sustained imbalance of supply (precipitation) and demand (i.e. evaporative demand). The demand side of drought is often overlooked but can be equally important as supply. In addition to common supply and demand drought indices available on Climate Engine (Table 1), the Evaporative Demand Drought Index (EDDI;

Hobbins et al., 2016; McEvoy et al., 2016) is also available, and computed with meteorological forcings from gridMET data (Abatzoglou, 2013) as inputs to the American Society of Civil Engineers Penman-Monteith standardized reference ET ($ET_0$) equation (ASCE-EWRI, 2005). EDDI is an effective drought metric due to two distinct feedbacks between regional evapotranspiration (ET) and $ET_0$: a complementary relationship under water-limited conditions (extended drought) where ET and $ET_0$ vary in opposite directions (Bouchet, 1963; Morton, 1969), and a parallel relationship under energy-limited conditions and at the onset drought (Budyko, 1974; Hobbins et al., 2016).

The summer of 2012 Great Plains drought stands out as one of the most extreme drought events in instrumental records (Hoerling et al., 2014), with estimated total economic losses (largely from the agriculture sector) of $35 billion U.S. dollars. The Climate Engine derived JJA EDDI map shown in Figure 3a highlights the large spatial extent of this drought, with extreme and exceptional drought categories stretching from the Canadian to Mexican borders and encompassing approximately two-thirds of the Continental U.S. Using the inter-annual time series options and spatial averaging feature of Climate Engine, the time series illustrated in Figure 3b shows the accumulated summer $ET_0$ anomaly averaged over Missouri in 2012 was greater than 200mm above average and approximately 100 mm greater than the previous record set in 1980.

MODIS Normalized Difference Vegetation Index (NDVI) and LST anomalies are especially useful for evaluating regional vegetation stress due to drought. During the warm season, LST is largely a function of the ET rate due to evaporative cooling (i.e. latent heat flux). If ET is relatively low, then the LST will be relatively high, and vice versa. Figures 3c-d illustrate reduced NDVI and increased LST during the summer of 2012 Great Plains drought due to reduced vegetation vigor and ET, respectively. Having multiple indicators of drought that are readily accessible through on-demand cloud computing and web visualization is extremely useful for better understanding the drivers and impacts of drought from multiple perspectives and disciplines (i.e. land surface energy balance, vegetation, near surface boundary layer).

Snow drought is a term that has been recently used to describe the lack of snow depth or coverage that occurs simultaneously with near normal or above normal precipitation conditions. A snow drought occurred during the winter and spring of 2014-2015 over the Northwestern U.S., featuring record low snowpack conditions in the Cascade and Northern Rocky Mountains even though respective precipitation amounts in many areas were at or above normal (Cooper et al., 2016; McEvoy et al., 2016). To illustrate this example, maps of the Standardized Precipitation Index (SPI; McKee et al., 1993), EDDI, and MODIS derived Normalized Difference Snow Index (NDSI) anomaly for December, 2014 - March, 2015 were generated with Climate Engine (Figures 4a-c).

### ***Fire***

Fire danger indices are used operationally to assess wildfire potential for short-term wildland fire business decision making (e.g., large fire potential) and used by the research community as a numerical measure of fuel aridity. Four sets of fire danger indices using the US National Fire Danger Rating System (Cohen and Deeming, 1985) are computed daily from the gridMET data and available via Climate Engine including the Energy Release Component (ERC). ERC is a proxy for daily potential fire radiative energy that integrates temperature, precipitation, humidity and solar radiation over the preceding several weeks which exhibits strong links to the occurrence of very large fires (Riley et al., 2013) and seasonal burned area (Abatzoglou and Williams, 2016), particularly across forested regions. A map of ERC anomalies and a time series of ERC averaged over Boise County, Idaho for JJA 2016 are shown in Figure 5a-b, respectively. The Pioneer Fire started on 18 July 2016 in the Boise National Forest and burned a total of 76 thousand hectares, making it one of the largest fires of the 2016 western U.S. fire season. The fire primarily burned during a period of well above normal ERC values for much of the latter half of July and August, including making large fire runs during the first couple days of August and last couple days of August when ERC values were well above normal approaching the 90-95th percentile for the calendar day. To visualize the areal extent of the burn, Figure 5c illustrates the 30-m pixel resolution Landsat 8 NDVI anomaly from July 18 to Sept. 22, 2016 relative to the Landsat 5, 7, and 8 climatology (1984-2015), clearly highlighted burned area as regions of decreased vegetation greenness.

### *Ecology*

The use of gridded climate and remote sensing products within the ecology community is becoming commonplace as relevant datasets have become available and accessible, and as requirements for long-term monitoring are becoming standard for permitting land and water development projects. Ecological modeling and monitoring typically requires fine scale information at long time scales (i.e. ~30+ yrs). The combination of gridded high-resolution climate data and the Landsat satellite image archive have catapulted ecological focused research, such as change detection at fine and large spatial scales (Cohen and Goward, 2004; Wulder et al., 2012; Roy et al., 2016).

Long-term monitoring of groundwater dependent ecosystems (GDEs) for baseline assessments and water and land use impacts analyses is a central focus area for many western U.S. federal, state, and non-governmental agencies. These agencies must adhere to regulations and requirements including environmental assessments and monitoring related to sage-grouse habitat, groundwater development, and mining. A compelling example of how Climate Engine can be used for advanced GDE monitoring is shown in Figure 6, which illustrates the coincident increase and decrease in Landsat derived summer vegetation vigor (i.e. NDVI) beginning in 2002 for respective agricultural and adjacent spring areas located in eastern Nevada and western Utah (Figures 6 b-c). These changes are a consequence of groundwater pumping for agriculture, lowering of the groundwater table, and drying of the spring (Halford, 2015; Huntington et al., 2016). Paired with gridMET water year precipitation and $ET_0$ computed with Climate Engine, Figure 6d shows that lowering of the groundwater table has markedly changed the vegetation response to precipitation within the spring area. Also evident is the complementary relationship between NDVI and $ET_0$ with PPT, a novel illustration showing how atmospheric demand, supply, and vegetation response are inherently linked.

***Agriculture***

Monitoring agricultural vegetation vigor is important for assessing water use, irrigation performance, crop yields, drought impacts, and for review and litigation of water rights, transfers, and disputes. All of these issues are receiving high priority attention in the western U.S. as well as in other water limited environments around the world. The use of high-resolution satellite imagery is needed to accurately characterize spatial and temporal variations in crop productivity, phenology, and water use over large areas. Given free access to the 30+ year Landsat archive combined with Google Earth Engine, rapid field scale assessments can be readily produced using Climate Engine.

An example of a field level analysis, where Climate Engine was used to generate maps of growing season maximum NDVI from Landsat for 2011 and 2015 over the Tulare Lake Basin, Central Valley of California, is shown in Figure 7. Figures 7a-b clearly illustrate the large amount of fallowing that occurred in 2015 due to the multiyear drought. Melton et al. (2015) estimated that over 2,000 $km^2$ of Central Valley cropland was fallowed in 2015, approximately twice that of 2011. A unique and very powerful feature of Climate Engine is the ability to extract field level time series information related to vegetation vigor for anywhere around the globe using predefined polygons, user-uploaded KML files, or by dynamically drawing polygons on the map to define areas of interest. The latter option is applied in Figure 7c to examine field level crop phenology stages (dormant, greenup, full cover, and senescence/harvest periods) from 2011-2015, clearly showing the fallowed land in 2015.

Africa's Sahel region is the semi-arid zone just south of the Sahara desert, but north of the humid tropical Africa. The agriculture, livestock and human villages and pastoralists in this region are heavily dependent on rainfall. During late 2015 to early 2016, a strong El Niño contributed to regional shifts in precipitation in the Sahel region. Significant drought across Ethiopia resulted in widespread crop failure and more than 10 million people in Ethiopia required food aid (U.S. Department of State, 2016). Global precipitation datasets can be used to detect local to regional anomalies in precipitation as a tool for devising early warning systems for drought related impacts such as famine. Whereas most available global precipitation products have coarse spatial resolutions, the Climate Hazards Group Infrared Precipitation with Stations (CHIRPS) dataset (Funk et al., 2015) provides quasi-global (50°S–50°N, 180°E–180°W) pentad (5-day) precipitation totals at ~4.8-km resolution from 1980-present, and is ideal for monitoring shifts in regional precipitation and drought in areas with limited observations such as Africa.

Climate Engine derived precipitation anomalies from CHIRPS for late 2015-early 2016 depict large portions of Ethiopia, particularly pastoral regions, received less than half of average rainfall during their primary growing season (Figure 8a). The multi-scalar and multi-product nature of Climate Engine is demonstrated by evaluating NDVI anomalies at regional and field scales with MODIS and Landsat datasets, respectively (Figures 8b-c), and is especially useful for supporting famine early warning efforts and assessments of on-the-ground impacts.

## Discussion and Conclusions

Cloud computing of environmental datasets are rapidly changing the way researchers and practitioners are conducting research, making applications, and planning for long-term application sustainability (Zhang et al., 2010; Hansen et al., 2013; Pekel et al., 2016; Yang et al., 2017). The motivation behind Climate Engine is to enable users to quickly process and visualize large datasets of climate and satellite earth observations for advanced monitoring and process understanding, and to improve early warning of drought, wildfire, and crop-failure risk at spatial scales relevant to scientists and decision-makers alike. Application features include on-demand mapping of environmental monitoring datasets, customizable analyses, time series and statistical summaries, downloadable digital data and URL link sharing that reproduce results in real-time.

What makes Climate Engine unique is the unprecedented access for processing, visualizing, and analyzing earth observation datasets with a simple web-connection, overcoming computational burdens of big data, and providing the ability to download or share results instead of downloading and processing entire data archives. A valid argument is that the science community should be focused on data discovery, providing answers, and creating new useful tools, rather than devoting time downloading and processing entire archives on local or research institution network computers. Cloud computing platforms, such as Google Earth Engine, allows us to move from archives to answers very efficiently, bypassing all the downloading and processing paralysis of yesteryear.

A primary challenge is integrating new cloud based research findings, products, and applications into decision making activities. The modular nature of Climate Engine allows for easy integration of additional climate and remotely sensed datasets that are added to Google Earth Engine collections. Future directions of Climate Engine involve working with collaborators to identify and integrate additional spatial averaging domains (e.g. watershed boundaries, grazing allotments, ecological units) for generating summary products, developing climate and remotely sensed datasets that best address community needs, and performing extensive and detailed outreach, stakeholder engagement, and trainings. Such stakeholder engagement and co-production of knowledge will ultimately enhance Climate Engine as a sustainable resource for advanced natural resource monitoring and process understanding, and to take the next step - translate data to decisions.

**Acknowledgements**

Funding for this study was provided by a Google Earth Engine faculty research award, and U.S. Geological Survey 2012–2017 Landsat Science Team, U.S. Bureau of Land Management Nevada State Office, U.S. Geological Survey - Great Basin Cooperative Ecosystem Study Unit, and National Oceanic and Atmospheric Administration – National Integrated Drought Information System grants. The authors would like to thank FEWS NET and the Climate Hazard Group at University of California, Santa Barbara, for their assistance in making CHIRPS precipitation products available through Google Earth Engine, and providing input on famine early warning applications.

**References**

Abatzoglou, J. T., 2013: Development of gridded surface meteorological data for ecological applications and modelling. *Int. J. Climatol.*, **33**(1), 121-131, doi: 10.1002/joc.3413.

Abatzoglou, J. T., and C. A. Kolden, 2013: Relationships between climate and macroscale area burned in the western United States. *Int. J. Wildland Fire*, **22**(7), 1003-1020, doi: 10.1071/WF13019.

Abatzoglou J. T., and A. P. Williams, 2016: The impact of anthropogenic climate change on wildfire across western US forests, *Proc. Natl. Acad. Sci.,* **113**(42), 11770-11775.

Anderson, M. C., J. M. Norman, J. R. Mecikalski., J. A. Otkin, and W. P. Kustas, 2007b: A climatological study of evapotranspiration and moisture stress across the continental United States based on thermal remote sensing: 2. Surface moisture climatology. J. Geophys. Res.: Atm., **112**(D11), doi: 10.1029/2006JD007506.

ASCE-EWRI., 2005: The ASCE standardized reference evapotranspiration equation, report 0-7844-0805-X, ASCE task committee on standardization of reference evapotranspiration, Reston, Virginia, *American Society of Civil Engineers*. (Available at) http://www. kimberly.uidaho.edu/water/asceewri/

Baumann, P., P., Mazzetti, J., Ungar, R., Barbera, D., Barboni, A., Beccati, and ...P. Campalani, 2016: Big data analytics for earth sciences: the earthserver approach. *International Journal of Digital Earth*, ***9***(1), 3-29.

Berrick, S.W., G. Leptoukh, J.D. Farley, and H. Rui, 2009. Giovanni: A Web Services Workfow-Based Data Visualization and Analysis System. IEEE Transactions on Geoscience and Remote Sensing **47**(1):106-113, DOI: 10.1109/TGRS.2008.2003183.

Bouchet, R. J., 1963: Evapotranspiration réelle et potentielle, signification climatique. *IAHS Publ*, *62*, 134-142.

Budyko, M. I., 1974: Climate and Life. International Geophysics Series, Vol. 18, Academic Press, 508 pp.

Brown, J. F., B. D. Wardlow, T. Tadesse, M. J. Hayes, and B. C. Reed, 2008: The Vegetation Drought Response Index (VegDRI): A new integrated approach for monitoring drought stress in vegetation. *GIsci Remote Sens.*, **45**(1), 16-46, doi: 10.2747/1548-1603.45.1.16.

Cohen J.E. and J. D. Deeming, 1985: The National Fire-Danger Rating System: basic equations. *Gen Tech Report* 16.

Cohen, W. B., and S. N. Goward, 2004: Landsat's role in ecological applications of remote sensing. *BioScience*, **54**(6), 535-545, doi: 10.1641/0006-3568(2004)054[0535:LRIEAO]2.0.CO;2.

Cooper, M. G., A. W. Nolin, and M. Safeeq, 2016: Testing the recent snow drought as an analog for climate warming sensitivity of Cascades snowpacks. *Environ. Res. Lett.*, **11**(8), 084009, doi: 10.1088/1748-9326/11/8/084009.

Daly, C., R. P. Neilson, and D. L. Phillips, 1994: A statistical-topographic model for mapping climatological precipitation over mountainous terrain. *J. Appl. Meteorol*., **33**(2), 140-158, doi: *10.1175/1520-0450(1994)033<0140:ASTMFM>2.0.CO;2*.

Eberle, J., S., Clausnitzer, C., Hüttich, and C., Schmullius, 2013: Multi-source data processing middleware for land monitoring within a web-based spatial data infrastructure for Siberia. *ISPRS International Journal of Geo-Information*, **2**(3), 553-576.

Funk, C., P. Peterson, M. Landsfeld, D. Pedreros, J. Verdin, S. Shukla, ... and J. Michaelsen, 2015: The climate hazards infrared precipitation with stations—a new environmental record for monitoring extremes. *Sci. Data*, 2, doi: 10.1038/sdata.2015.66.

Hall, D. K., J. C. Comiso, N. E. DiGirolamo, C. A. Shuman, J. E. Box, and L. S. Koenig, 2013: Variability in the surface temperature and melt extent of the Greenland ice sheet from MODIS. *Geophys. Res. Lett*., **40**(10), 2114-2120, doi: 10.1002/grl.50240.

Hansen, M. C., P. V. Potapov, R. Moore, M. Hancher, S. A. Turubanova, A. Tyukavina, ... and A. Kommareddy, 2013: High-resolution global maps of 21st-century forest cover change. *Science*, 342(6160), 850-853, doi: 10.1126/science.1244693.

Halford, K.J., 2015: Exhibit 153, public administrative hearing before the state engineer in the matter of protested applications 78795, etc., February 2–6, 2015, official records in the Office of the Nevada State Engineer.

Hobbins, M. T., D. J. McEvoy, J. L. Huntington, C. Morton, and J. Verdin, 2016: The Evaporative Demand Drought Index. Part I: Linking drought evolution to variations in evaporative demand. *J. Hydrometeor.*, 17, 1745–1761, doi:10.1175/ JHM-D-15-0121.1.

Hoerling, M., J. Eischeid, A. Kumar, R. Leung, A. Mariotti, K. Mo, ... and R. Seager, 2014: Causes and predictability of the 2012 Great Plains drought. *Bull. Am. Meteorol. Soc.*, **95**(2), 269-282, doi: *10.1175/BAMS-D-13-00055.1*.

Huntington, J., K. McGwire, C. Morton, K. Snyder, S. Peterson, T. Erickson., ... and R. Allen, 2016: Assessing the role of climate and resource management on groundwater dependent ecosystem changes in arid environments with the Landsat archive. *Remote Sens. Environ.,* 185, 186-197, doi:10.1016/j.rse.2016.07.004.

McEvoy, D. J., J. L. Huntington, M. T. Hobbins, A. Wood, C. Morton, J. Verdin, ... and C. Hain, 2016: The Evaporative Demand Drought Index: Part II–CONUS-wide

Assessment Against Common Drought Indicators. *J. Hydrometeorol.*, doi: *10.1175/JHM-D-15-0122.1*.

McKee, T. B., N. J. Doesken, and J. Kleist, 1993: The relationship of drought frequency and duration to time scales. Preprints, Eighth Conf. on Applied Climatology, Anaheim, CA, *Amer. Meteor. Soc*., 179–184.

Melton, F., C. Rosevelt, A. Guzman, L. Johnson, and I. Zargoza, 2015: Fallowed Area Mapping for Drought Impact Reporting: 2015 Assessment of Conditions in the California Central Valley, Fallowed Area Mapping for Drought Impact Reporting and Decision Making Report, October 14, 2015, https://nex.nasa.gov/nex/resources/371/.

Mitchell, K. E., D. Lohmann, P. R. Houser, E. F. Wood, J. C. Schaake, A. Robock, ... and R. W. Higgins, 2004: The multi-institution North American Land Data Assimilation System (NLDAS): Utilizing multiple GCIP products and partners in a continental distributed hydrological modeling system. *J. Geophys. Res.: Atm.*, **109**(D7), doi: 10.1029/2003JD003823.

Moore, R. T., and M. C. Hansen, 2011: Google Earth Engine: A new cloud-computing platform for global-scale earth observation data and analysis. American Geophysical Union Fall Meeting Abstracts. 1: p. 02.

Morton, F. I. (1969). Potential evaporation as a manifestation of regional evaporation. *Water Resour. Res.*, **5**(6), 1244-1255.

Mottram,R. Unusually Early Greenland Melt. Polar Portal: monitoring ice and climate in the arctic.http://polarportal.dk/en/nyheder/arkiv/nyheder/usaedvanlig-tidlig-afsmeltning-i-groenland/. April 12, 2016.

Nghiem, S. V., Hall, D. K., Mote, T. L., Tedesco, M., Albert, M. R., Keegan, K., ... and G. Neumann, 2012: The extreme melt across the Greenland ice sheet in 2012. *Geophys. Res. Lett.*, **39**(20), doi: 10.1029/2012GL053611.

Nicholson, S. E., 2013: The West African Sahel: A review of recent studies on the rainfall regime and its interannual variability. *ISRN Meteorology*, 2013, 32p., doi: 10.1155/2013/453521.

Overland, J. E., and M. Wang, 2016: Recent Extreme Arctic Temperatures are due to a Split Polar Vortex. *J. Clim*., **29**(15), 5609-5616, doi: *10.1175/JCLI-D-16-0320.1*.

Oyler, J.W., A. Ballantyne, K. Jencso, M. Sweet, and S. W. Running, 2014: Creating a topoclimatic daily air temperature dataset for the conterminous United States using homogenized station data and remotely sensed land skin temperature. *Int. J. Climatol.*, **35**(9), 2258-2279, doi:10.1002/joc.4127,

Pekel, J. F., A., Cottam, N., Gorelick, and A. S. Belward, 2016: High-resolution mapping of global surface water and its long-term changes. *Nature*, doi:10.1038/nature20584.

Pettorelli, N., J. O. Vik, A. Mysterud, J. M. Gaillard, C. J. Tucker, and N. C. Stenseth, 2005: Using the satellite-derived NDVI to assess ecological responses to environmental change. *Trends Ecol. Evol.*, **20**(9), 503-510, doi: 10.1016/j.tree.2005.05.011.

Riley, K. L., J. T. Abatzoglou, I. C. Grenfell, A. E. Klene, and F. A. Heinsch, 2013: The relationship of large fire occurrence with drought and fire danger indices in the western USA, 1984–2008: the role of temporal scale. *Int. J. Wildland Fire,* **22**(7), 894-909, doi: 10.1071/WF12149.

Roy, D. P., M. A. Wulder, T. R. Loveland, C. E. Woodcock, R. G. Allen, M. C. Anderson, M. C., ... and T. A. Scambos, 2014: Landsat-8: Science and product vision for terrestrial global change research. *Remote Sens. Environ.*, 145, 154-172, doi: 10.1016/j.rse.2014.02.001.

Saha, S., S. Moorthi, H. L. Pan, X. Wu, J. Wang, S. Nadiga, ... and H. Liu, 2010: The NCEP climate forecast system reanalysis. *Bull. Am. Meteorol. Soc.*, **91**(8), 1015, doi: *10.1175/2010BAMS3001.1* .

Sun, L., Perlwitz, J., and M. Hoerling, 2016: What caused the recent "Warm Arctic, Cold Continents" trend pattern in winter temperatures? *Geophys. Res. Lett.*, doi: 10.1002/2016GL069024.

Svoboda, M., and Coauthors, 2002: The Drought Monitor. *Bull. Amer. Meteor. Soc*., 83, 1181–1190, doi:10.1175/ 1520-0477(2002)083,1181:TDM.2.3.CO;2.

Teng, W., H., Rui, R., Strub, and B., Vollmer, 2016: Optimal Reorganization of NASA Earth Science Data for Enhanced Accessibility and Usability for the Hydrology Community. *JAWRA Journal of the American Water Resources Association*, *52*(4), 825-835.

Thornton, P. E., M. M. Thornton, B. W. Mayer, N. Wilhelmi, Y. Wei, R. Devarakonda, and R. B. Cook, R. B., 2014: Daymet: Daily Surface Weather Data on a 1-km Grid for North America, Version 2. Oak Ridge National Laboratory (ORNL), doi: 10.3334/ORNLDAAC/1219.

U.S. Department of State. 2016. Briefing on Announcement of New Measures to Address the Drought in Ethiopia. http://www.state.gov/r/pa/prs/ps/2016/03/253954.htm

Wang, L., and J. J. Qu, 2007: NMDI: A normalized multi-band drought index for monitoring soil and vegetation moisture with satellite remote sensing.*Geophys. Res. Lett.,* 34(20), doi: 10.1029/2007GL031021.

Waugh, D. W., A. H. Sobel, and L. M. Polvani, 2016: WHAT IS THE POLAR VORTEX, AND HOW DOES IT INFLUENCE WEATHER?. *Bull. Am. Meteorol. Soc.*, (2016), doi: 10.1175/BAMS-D-15-00212.1 .

Wulder, M. A., J. G. Masek, W. B. Cohen, T. R. Loveland, and C. E. Woodcock, 2012: Opening the archive: How free data has enabled the science and monitoring promise of Landsat. *Remote Sens. Environ.*, 122, 2-10, doi: 10.1016/j.rse.2012.01.010.

Yang, C., M., Yu, F., Hu, Y., Jiang, and Y., Li, 2017: Utilizing Cloud Computing to address big geospatial data challenges. *Computers, Environment and Urban Systems*, *61*, 120-128.

Zhang, Q., L. Cheng, and R. Boutaba, 2010: Cloud computing: state-of-the-art and research challenges. *Journal of internet services and applications*, 1(1), 7-18, doi: 10.1007/s13174-010-0007-6.

***Sidebar 1 - Application Development and Design***

The Climate Engine web application is hosted on the Google App Engine web server, while the source code is hosted on a GitHub repository for version control and source code management. The source code is divided into two parts: the front-end that the user sees on the web page and the back-end where the data requested is formed and processed.

The front-end display of Climate Engine is viewed in a web browser and is constructed using the Twitter Bootstrap3 CSS (Cascading Style Sheets) web framework for the navigation bars and tabs, and the overall responsive design of the site. The display contains a form for the user to customize their request and a section for displaying the response (a map layer or a time series figure with data).

The back-end of Climate Engine utilizes Google's webapp2 Python web framework and functions from Google’s Earth Engine Python API to create the custom data extraction and processing request for Earth Engine. The request is submitted as an AJAX (Asyhchronous JAvascript and XML) request to Earth Engine. On Earth Engine servers, the data is extracted from the Google Cloud and processed in parallel. Earth Engine sends back a response to the Climate Engine application as map ids for the map layers, JSON (JavaScript Object Notation) data for the time series, and URL links for map downloads. For time series requests, the returned data in JSON format is processed into JavaScript arrays for creating HighCharts figures. For map requests the Google map display is parsed into tiles and a URL request (containing the map id) is sent to Earth Engine to compute the layer at the resolution needed for display. As the user zooms in on the Google map, the computations needed to further refine the spatial resolution of the map layers are performed on Earth Engine in real-time, and are reloaded on the user’s map.

The map layer display illustrates user-requested raster output on a Google map. Climate Engine provides the ability for the user to customize the map layer (e.g. scale and color palette options) and to place optional vector images (e.g. KML, polygons, Google Fusion Tables) atop the map layer to aid in geographical orientation, or to be used for spatial averaging.

The time series display illustrates a time series figure and respective data as a tabular list alongside the figure. The figure is a scalable vector graphic (SVG) constructed using the HighCharts JavaScript graphics library, which displays the user-requested data in an interactive figure. Climate Engine provides the ability for the user to customize the time series figure (e.g. scatter, bar, or line charts) on the fly without resubmitting the request.

The beauty of this application framework is that the requests can be made from anywhere a web browser has an internet connection, all major computing is performed using the thousands of processors via Earth Engine, and results are returned to the device for display and/or download.

**List of Figure Captions**

Figure 1. User interface of Climate Engine illustrating the (top) mapping, and (bottom) time series menus. The spatial distribution of average latent heat flux (LE) from Climate Forecast System Reanalysis (CFSR) for July 23-September 20, 2016 is displayed using user defined colormap options (top). A time series of spatially averaged daily LE is displayed in (b) for July 23-September 20, 2016 for a user-drawn polygon over the western US (shown in blue in top figure).

Figure 2. Land surface temperature (LST) anomalies from MODIS for (a) January - February, 2016, (b) January - March, 2015, and (c) and April 2016 relative to 2000-2015 averages extracted from Climate Engine's mapping tools. Figures illustrate patterns of anomalously warm and cool temperatures over the Arctic and mid-latitude continents, respectively, potentially caused by a combination sea-ice loss and internal atmospheric variability. Panel (d) shows the Normalized Difference Snow Index (NDSI) anomaly from MODIS for April 2016 for southern Greenland, where unusually warm temperatures resulted in an unusually early melting in south-western Greenland.

Figure 3. Effects of the 2012 Great Plains drought on near surface boundary layer feedbacks between ET and $ET_0$ are shown through maps of (a) June - August EDDI, (c) MODIS NDVI, and (d) LST anomalies relative to 2000-2015 averages extracted from Climate Engine's mapping tool. Panel (b) shows a time series of accumulated JJA

Penman-Monteith reference $ET_0$ averaged over the state of Missouri from 1979-2015 using Climate Engine’s time series tool.

Figure 4. The 2015 snow drought over the Northwestern U.S. is shown by Climate Engine generated maps of December 2014 - March 2015 (a) SPI, (b) EDDI, and (c) MODIS Normalized NDSI anomalies relative to 2000-2015 averages. SPI shows little to no drought over the Cascades and Northern Rockies. However, EDDI shows extreme drought conditions primarily caused by anomalously high temperature and solar radiation. This led to extremely high freezing levels, resulting in anomalously low snow cover at mid to high elevations as illustrated by the NDSI anomaly.

Figure 5. Fire danger illustrated using the Energy Release Component (ERC) over the mountains of southwestern Idaho is illustrated with a Climate Engine generated (a) map of mean ERC values expressed as a percent departure from average for the May 1-September 5, 2016 relative to 1981-2010 normals, and (b) time series of daily ERC values averaged over Boise County, Idaho (outlined in black in panel (a)) for May 1-September 5, 2016 shown by the red trace, with 1979-2015 daily median values and daily 5-95th percentile shown by the black trace and grey shading, respectively. Panel (c) shows the Landsat NDVI anomaly for July 18 - September 22, 2016 relative to the Landsat 5/7/8 climatology (1984-2015) where the 76 thousand hectare Pioneer Fire occurred.

Figure 6. Effects of groundwater irrigation on spring area vegetation vigor in eastern Nevada and western Utah are illustrated using the time series tool of Climate Engine to track August - September average NDVI from 1984-2016 spatially averaged over two user-drawn domains highlighted in (a). Irrigation commenced in 2002 resulting in (b) increased NDVI and a coincident (c) decline in NDVI within the spring area due to lowering of the groundwater table and drying of the spring. Lowering of the groundwater table changed the vegetation response to precipitation within the spring area as evidenced by (d) pre- and post-irrigation NDVI and water year precipitation (PPT) relationships.

Figure 7. Extensive fallowed cropland in 2015 within the Tulare Lake Basin, Central Valley of California, due to multiyear drought is illustrated with the spatial distribution of Landsat growing season (April - October) maximum NDVI for (a) 2011 and (b) 2015. (c) The time series tool in Climate Engine was used to extract NDVI from 2011-2015 for the red polygon illustrated in panels (a-b). Field level crop phenology stages (identified as a cotton crop for all years according to USDA cropland data layers) are clearly evident, along with fallowing that occurred in 2015.

Figure 8. (a) The September 2015-February 2016 CHIRPS precipitation anomaly over Africa relative to 1981-2010 conditions depict large areas of Ethiopia received less than half of normal precipitation. Consequently, widespread impacts to agricultural productivity, especially within pastoral regions, were present across Ethiopia evidenced by reduced greenness in remote sensing images. (b) MODIS NDVI anomalies for

September 2015-February 2016 relative to 2000-2015 normals are shown for the inset box of panel (a). (c) Landsat NDVI anomalies for September 2015-February 2016 relative to 2000-2015 normals are shown for the inset box of panel (b).

## List of Table Captions

Table 1. Satellite and climate datasets and respective variables currently available in Climate Engine. Additional datasets, variables, and calculations will be added as Climate Engine evolves.

## Figures and Caption

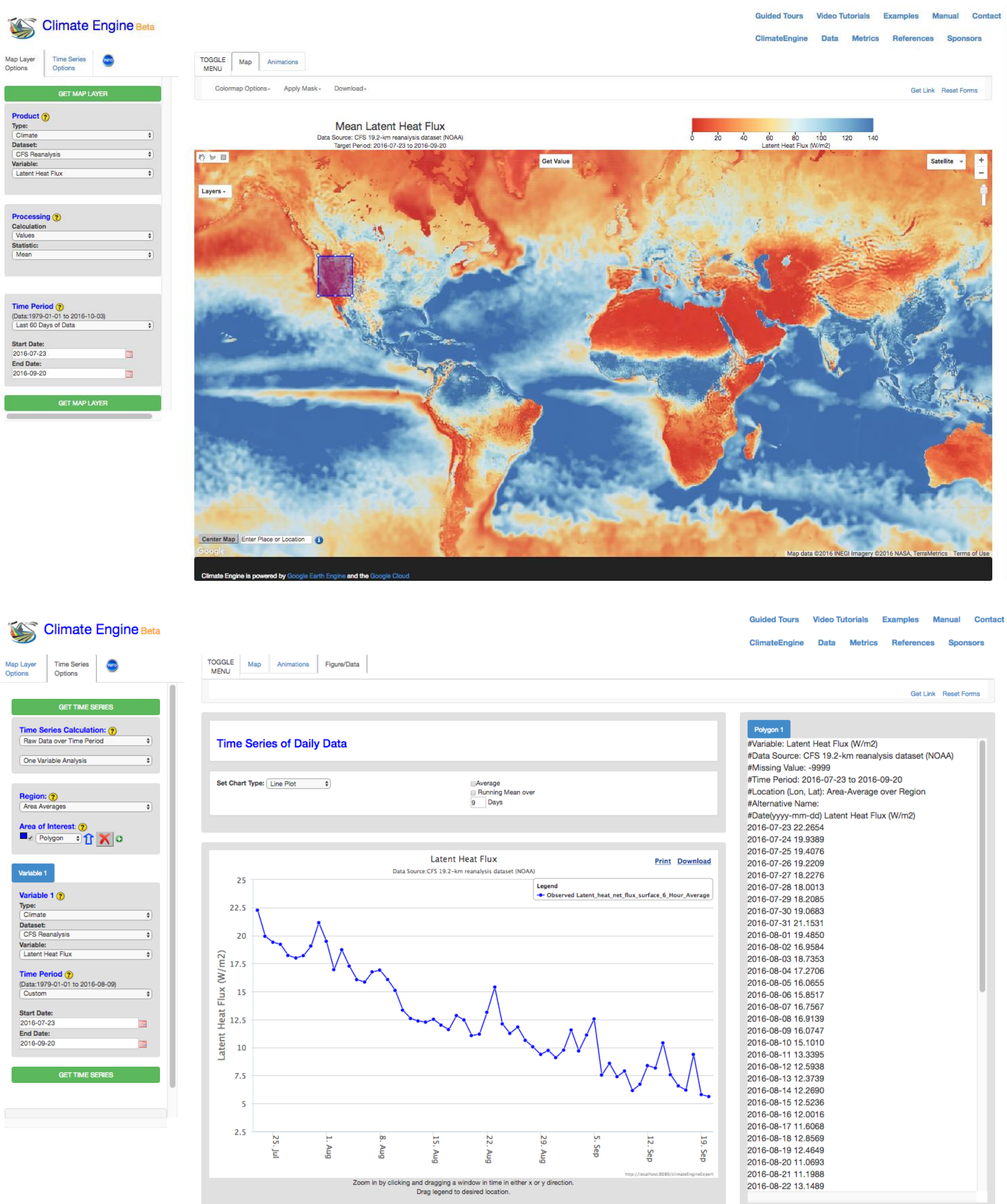


Figure 1. User interface of Climate Engine illustrating the (top) mapping, and (bottom) time series menus. The spatial distribution of average latent heat flux (LE) from Climate

Forecast System Reanalysis (CFSR) for July 23-September 20, 2016 is displayed using user defined colormap options (top). A time series of spatially averaged daily LE is displayed in (b) for July 23-September 20, 2016 for a user-drawn polygon over the western US (shown in blue in top figure).

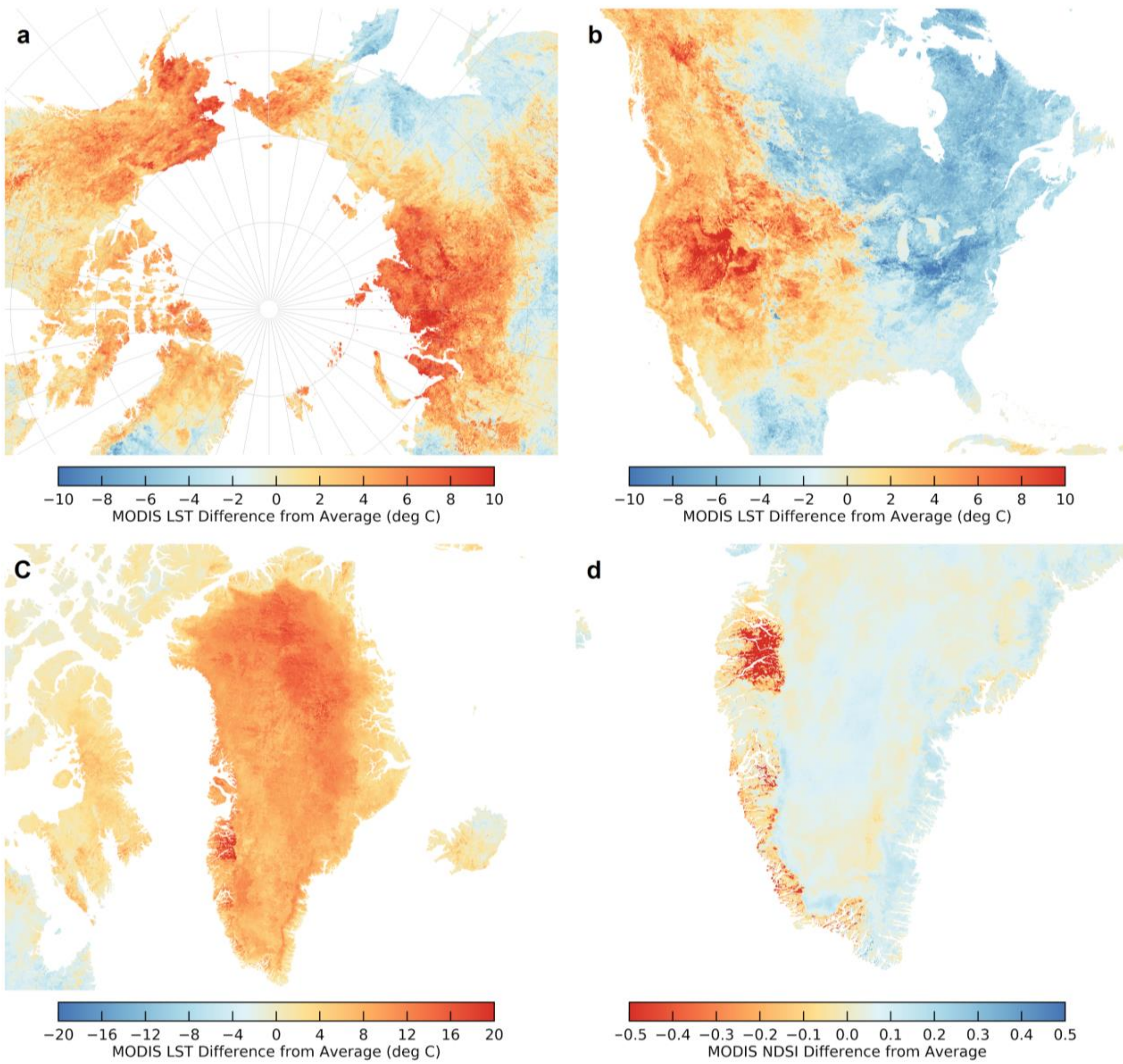


Figure 2. Land surface temperature (LST) anomalies from MODIS for (a) January - February, 2016, (b) January - March, 2015, and (c) and April 2016 relative to 2000-2015

averages extracted from Climate Engine's mapping tools. Figures illustrate patterns of anomalously warm and cool temperatures over the Arctic and mid-latitude continents, respectively, potentially caused by a combination sea-ice loss and internal atmospheric variability. Panel (d) shows the Normalized Difference Snow Index (NDSI) anomaly from MODIS for April 2016 for southern Greenland, where unusually warm temperatures resulted in an unusually early melting in south-western Greenland.

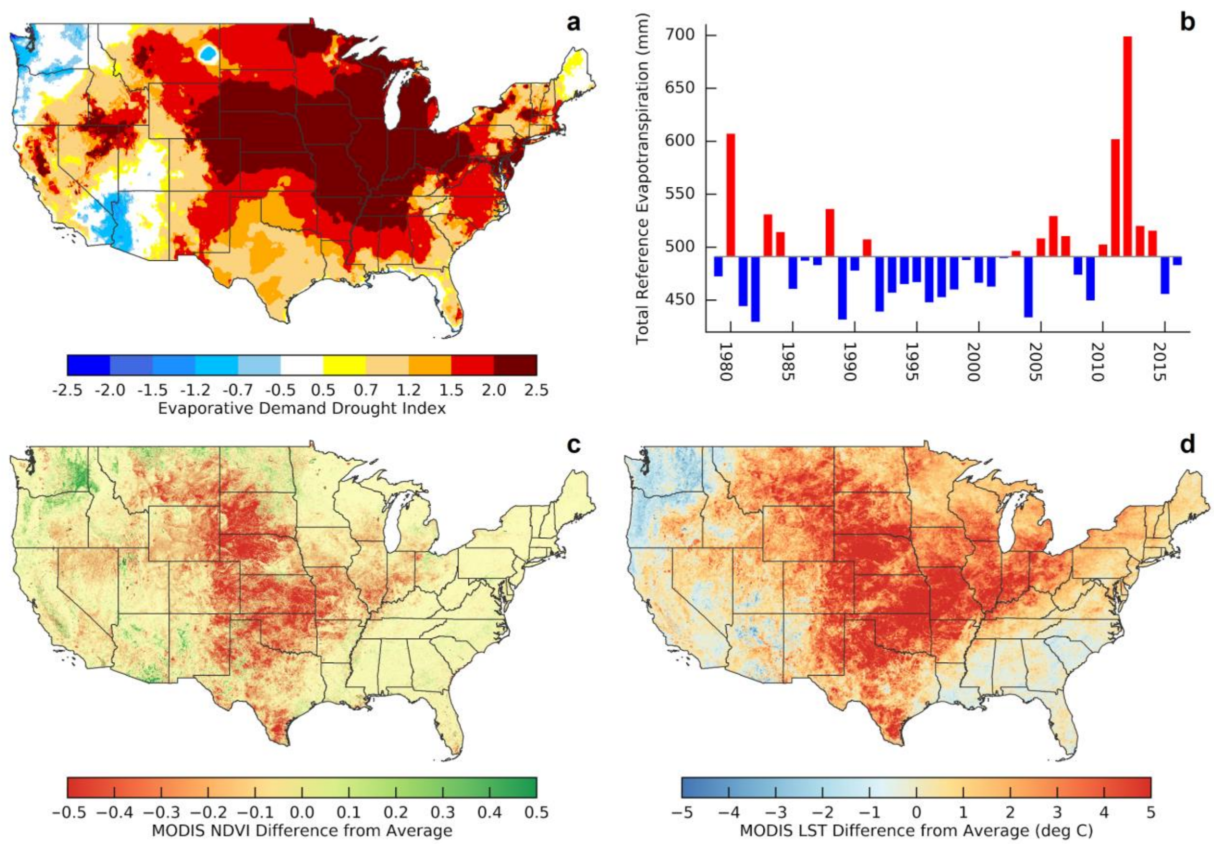


Figure 3. Effects of the 2012 Great Plains drought on near surface boundary layer feedbacks between ET and $ET_0$ are shown through maps of (a) June - August EDDI, (c) MODIS NDVI, and (d) LST anomalies relative to 2000-2015 averages extracted from Climate Engine's mapping tool. Panel (b) shows a time series of accumulated JJA

Penman-Monteith reference $ET_0$ averaged over the state of Missouri from 1979-2015 using Climate Engine's time series tool.

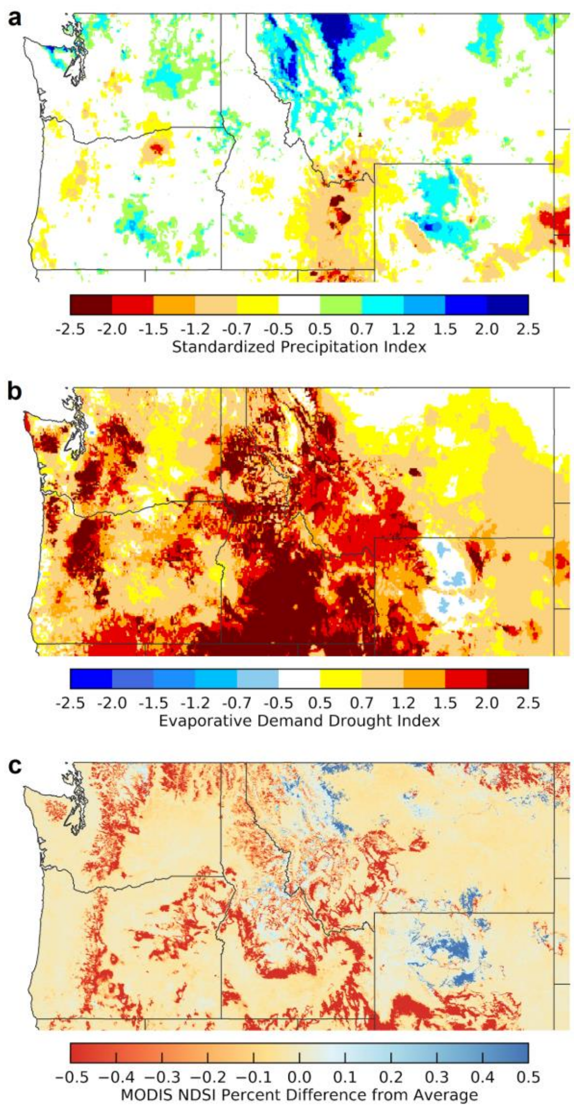


Figure 4. The 2015 snow drought over the Northwestern U.S. is shown by Climate Engine generated maps of December 2014 - March 2015 (a) SPI, (b) EDDI, and (c) MODIS Normalized NDSI anomalies relative to 2000-2015 averages. SPI shows little to no drought over the Cascades and Northern Rockies. However, EDDI shows extreme drought conditions primarily caused by anomalously high temperature and

solar radiation. This led to extremely high freezing levels, resulting in anomalously low snow cover at mid to high elevations as illustrated by the NDSI anomaly.

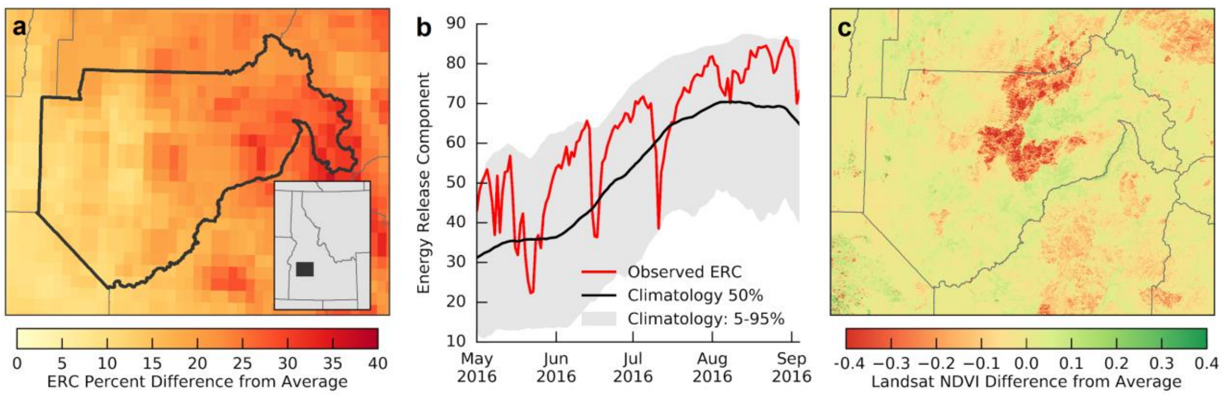


Figure 5. Fire danger illustrated using the Energy Release Component (ERC) over the mountains of southwestern Idaho is illustrated with a Climate Engine generated (a) map of mean ERC values expressed as a percent departure from average for the May 1-September 5, 2016 relative to 1981-2010 normals, and (b) time series of daily ERC values averaged over Boise County, Idaho (outlined in black in panel (a)) for May 1-September 5, 2016  shown by the red trace, with 1979-2015 daily median values and daily 5-95th percentile shown by the black trace and grey shading, respectively. Panel (c) shows the Landsat NDVI anomaly for July 18 - September 22, 2016 relative to the Landsat 5/7/8 climatology (1984-2015) where the 76 thousand hectare Pioneer Fire occurred.

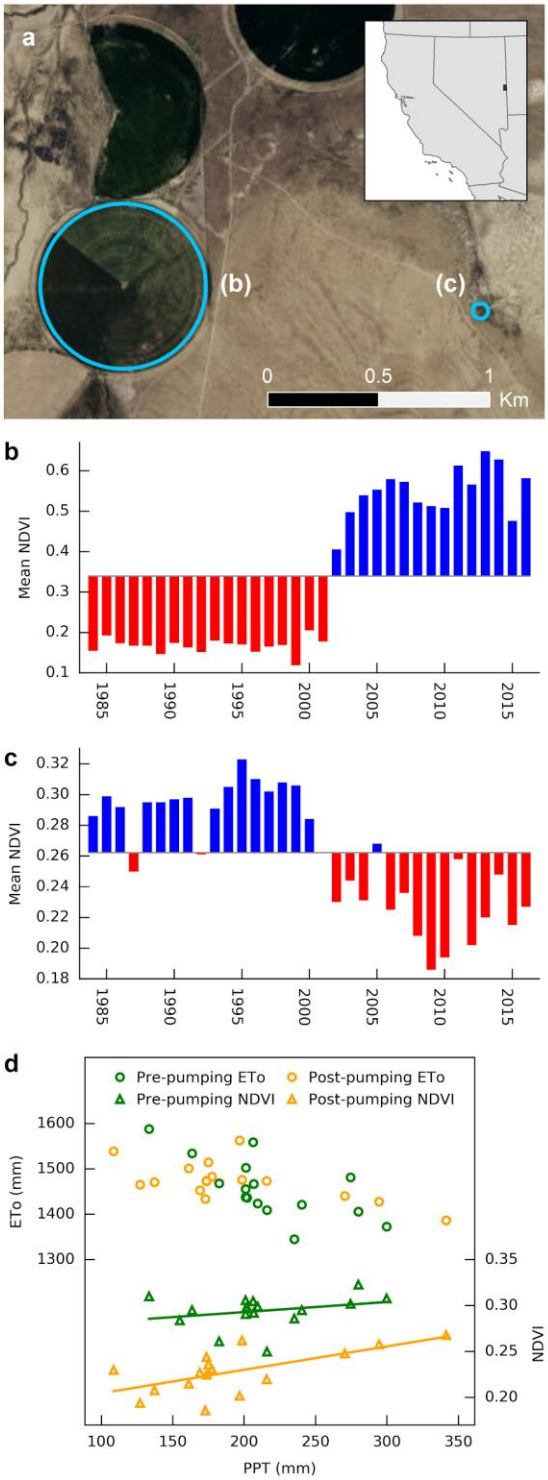


Figure 6. Effects of groundwater irrigation on spring area vegetation vigor in eastern Nevada and western Utah are illustrated using the time series tool of Climate Engine to track August - September average NDVI from 1984-2016 spatially averaged over two user-drawn domains

highlighted in (a). Irrigation commenced in 2002 resulting in (b) increased NDVI and a coincident (c) decline in NDVI within the spring area due to lowering of the groundwater table and drying of the spring. Lowering of the groundwater table changed the vegetation response to precipitation within the spring area as evidenced by (d) pre- and post-irrigation NDVI and water year precipitation (PPT) relationships.

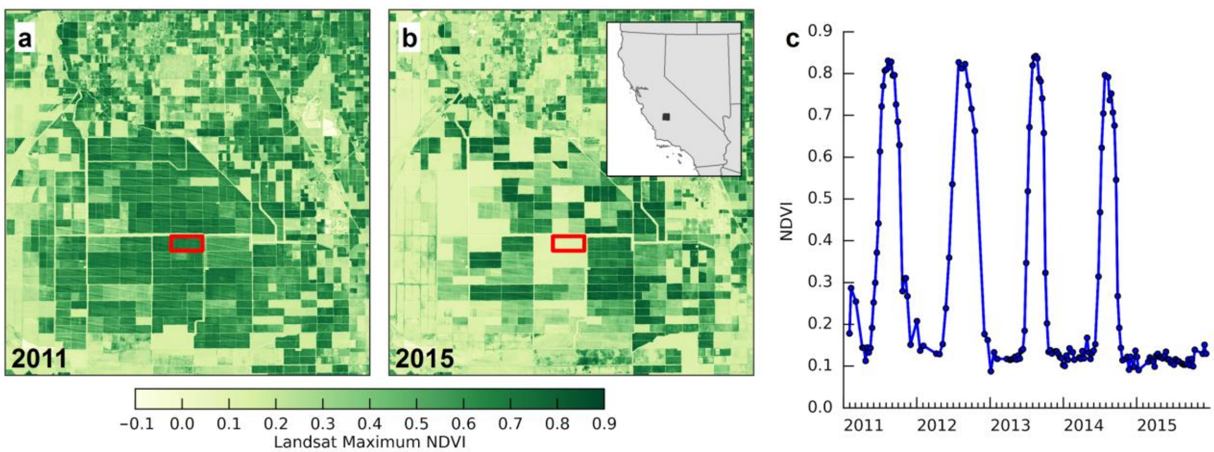


Figure 7. Extensive fallowed cropland in 2015 within the Tulare Lake Basin, Central Valley of California, due to multiyear drought is illustrated with the spatial distribution of Landsat growing season (April - October) maximum NDVI for (a) 2011 and (b) 2015. (c) The time series tool in Climate Engine was used to extract NDVI from 2011-2015 for the red polygon illustrated in panels (a-b). Field level crop phenology stages (identified as a cotton crop for all years according to USDA cropland data layers) are clearly evident, along with fallowing that occurred in 2015.

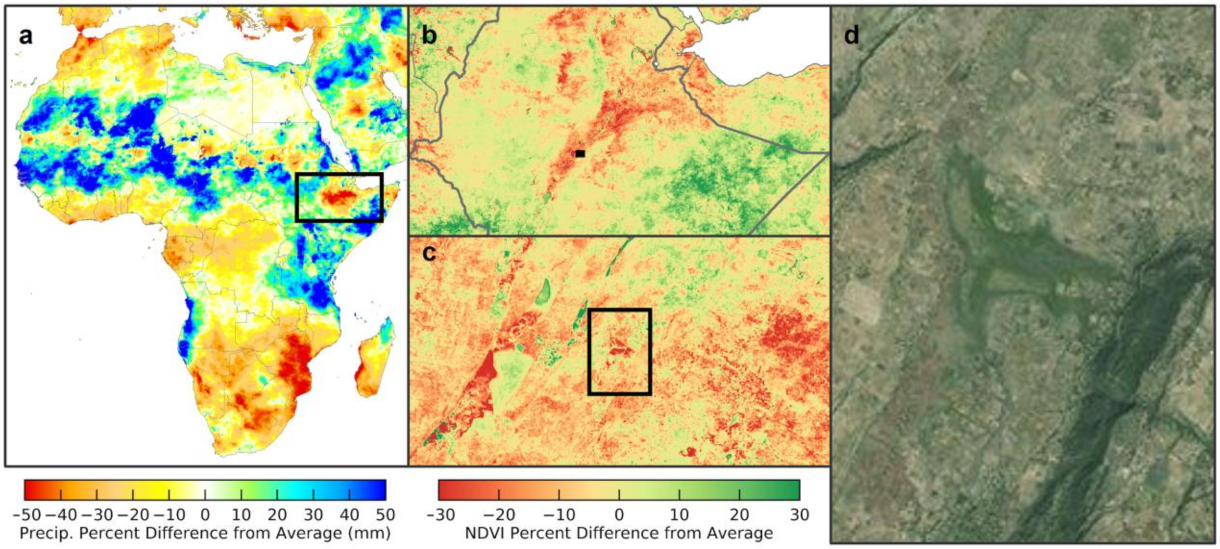


Figure 8. (a) The September 2015-February 2016 CHIRPS precipitation anomaly over Africa relative to 1981-2010 conditions depict large areas of Ethiopia received less than half of normal precipitation. Consequently, widespread impacts to agricultural productivity, especially within pastoral regions, were present across Ethiopia evidenced by reduced greenness in remote sensing images. (b) MODIS NDVI anomalies for September 2015-February 2016 relative to 2000-2015 normals are shown for the inset box of panel (a). (c) Landsat NDVI anomalies for September 2015-February 2016 relative to 2000-2015 normals are shown for the inset box of panel (b).

## Tables and Captions

Table 1. Satellite and climate datasets and respective variables currently available in Climate Engine. Additional datasets, variables, and calculations will be added as Climate Engine evolves.

| Satellite Data | Variables[1] | Spatial Resolution | Temporal Resolution | Duration | References | Google Earth Engine Asset Catalog |
|---|---|---|---|---|---|---|
| Landsat 4, 5, 7, 8 top-of-atmosphere and at-surface reflectance | LST, NDVI, EVI, NDSI, NDWI, NBRT, TC, FC, Blue, Green | 30-120m | 16 day | 1984-pres. | NASA/USGS | https://goo.gl/GFmZVg; https://goo.gl/SEzNsB |
| Terra/MODIS | LST, NDVI, EVI, NDSI, BAI, NDWI, FSC | 500-1000m | 8-16 day | 2000-pres. | NASA | https://goo.gl/kQpqfI |
| AVHRR-Pathfinder | SST | 4km | daily | 1981-2012 | NOAA | https://goo.gl/934c1g |
| **Climate Data** | **Variables[2]** | **Spatial Resolution** | **Temporal Resolution** | **Duration** | **References** | **Google Earth Engine Asset Catalog** |
| gridMET/METDATA | T, Rs, q, Td, U, ETo, P, PPT-ETo, BI, ERC, FM100, FM1000, PDSI, EDDI, SPI, SPEI | 4km | daily | 1979-pres. | Abatzoglou (2013) | https://goo.gl/17WF3c |
| CFSR | T,Rs, Rl, Rn, q, U, PET, P, LE, H, SM | ~19-29km | 6 hourly | 1979-pres. | Saha et al. (2010) | https://goo.gl/Kcy1MF |
| CHIRPS | P | 1km | 5 day | 1980-pres. | Funk et al. (2015) | https://goo.gl/eSEpr2 |

[1]Satellite Variables: LST, Land Surface Temperature; NDVI, Normalized Difference Vegetation Index; EVI, Enhanced Vegetation Index; NDSI, Normalized Difference Snow Index; NDWI, Normalized Difference Water Index; NBRT, Normalized Difference Burn Ratio Thermal Index; TC, True Color Composite; FC, False Color Composite; Blue, blue reflectance; Green, green reflectance; SST, Sea Surface Temperature

[2]Climate Variables: T, Temperature; Rs, downward solar radiation at the surface; q specific humidity; Td, dewpoint temperature; U, wind speed; ETo, ASCE reference ET; P, precipitation; PPT-ETo, potential water deficit; BI, Burning Index; ERC, Energy Release Component; FM100, 100-hr Dead Fuel Moisture; FM1000, 1000-hr Dead Fuel Moisture; PDSI, Palmer Drought Severity Index; EDDI, Evaporative Demand Drought Index; SPI, Standardized Precipitation Index; SPEI, Standardized Precipitation Evapotranspiration Index; Rl, downward longwave radiation at the surface; Rn, net radiation; LE, latent heat flux; H, sensible heat flux, SM soil moisture at 5, 25, 70, 150cm